# EFFECTS OF FREESTREAM TURBULENCE INTENSITY ON THE SPATIO-TEMPORAL CHARACTERISTICS OF FLOW SEPARATION AROUND RECTANGULAR PRISM

**Fati Bio Abdul-Salam**
Department of Mechanical Engineering
University of Manitoba
Winnipeg, MB R3T 5V6, Canada
abdulsa8@myumanitoba.ca

**Mark F. Tachie**
Department of Mechanical Engineering
University of Manitoba
Winnipeg, MB R3T 5V6, Canada
mark.tachie@umanitoba.ca

## ABSTRACT

The influence of freestream turbulence (FST) intensity on the flow dynamics around a rectangular prism was investigated using a time-resolved particle image velocimetry. Three FST intensities (Tu = 2%, 5%, and 13%) were examined at a Reynolds number (based on the prism thickness) of 10000. The mean flow reveals a monotonic decrease in the size of the recirculation bubble over the prism as FST intensity increases, but the wake bubble is independent of the FST intensity. The Kelvin–Helmholtz instability is observed near the leading edge for the Tu = 2% and 5% test cases at Strouhal numbers of 2.07 and 2.60, respectively, but it is bypassed in the Tu = 13% test case. The wake shedding frequency is independent of the FST intensity. The streamwise Reynolds normal stress increases significantly with an increase in FST intensity. Spectral decomposition analysis shows that increasing FST intensity reduces the small-scale contribution to the Reynolds stress.

## INTRODUCTION

Flow over bluff bodies with rectangular cross-sections is commonly used to study the complex dynamics of separated and reattached flows due to their geometric simplicity and relevance to a wide range of practical applications. The flow is characterized by small-scale Kelvin-Helmholtz (KH) instability, which originates from the roll-up of the separated shear layers formed at the leading edges of the prism. In the wake region, von Kármán (VK) vortices are formed due to the alternating signed vortices of equal strength shed along the prism centreline. The separated flow over the prism also features a large-scale unsteadiness, associated with low-frequency contraction/enlargement of the separation bubble (flapping motion) (Kiya and Sasaki, 1983; Abdul-Salam et al., 2024; Cimarelli et al., 2024). Thus, the flow is exemplified by three distinct instabilities namely KH, VK vortex shedding and low-frequency flapping motion.

Rectangular prisms are primarily defined by their chord-to-thickness ratio (CR = $C/h$, where $C$ and $h$ are, respectively, the chord length and thickness of the prism), which strongly affects the flow dynamics (Okajima, 1982; Moore et al., 2019). Flow parameters such as the Reynolds number (Re), blockage ratio, and freestream turbulence (FST) also affect the flow characteristics, with their degree of influence strongly dependent on the chord-to-thickness ratio (Okajima, 1982; Lander et al., 2016; Kumahor and Tachie, 2023; Abdul-Salam et al., 2024).

Most studies that investigated the flow dynamics around rectangular prisms were performed at low FST intensity (Tu ≤ 2%) to isolate its intrinsic effects on the flow dynamics. However, in many practical applications, high FST levels are prevalent due to factors such as atmospheric gusts and wakes from upstream structures. Previous studies on the effects of FST intensity have primarily focused on short prisms (CR < 2) or infinitely long prisms (CR > 16). For instance, Zhao et al. (2021) investigated the effects of FST intensity on the flow around a square prism (CR = 1) for Tu = 0.5%, 5.0% and 12.1%. For square prisms, the separated shear layers are shed directly into the wake without reattaching on the surface of the prism. They showed that increasing FST level promotes the tendency of the separated shear layers to reattach onto the surface of the prism, which in turn weakens the strength and coherence of the vortex shedding in the wake. A similar observation was made by Lander et al. (2016) and Li et al. (2022) for a square prism. On the effects of FST on infinitely long prisms, Kiya and Sasaki (1983) examined a prism with CR = 25 for Tu = 1% to 7%, and found that FST increases the curvature of the separated shear layer towards the surface of the prism and decreases the size of the recirculation bubble.

While these studies have improved our understanding of the effects of FST on the separated flow around rectangular prism, studies on intermediate prisms, which are representative of many practical engineering configurations such as cargo trucks, bridge decks, and rail cars remain limited. Given the strong dependence of flow dynamics on the chord-to-thickness ratio, it is imperative to examine the influence of FST on the unsteady dynamics and instabilities in separated flows over intermediate prisms.

Therefore, the objective of the present study is to investigate the effects of FST intensity on the spatial and temporal features of flow over a finite rectangular prism with CR = 6 using time-resolved particle image velocimetry (TR-PIV). The results are analyzed in terms of mean velocity, Reynolds stresses, and frequency spectra of the velocity fluctuations and reverse flow area. Spectral decomposition of the Reynolds stresses is used to examine the contributions of the different instabilities under varying FST intensities.

## EXPERIMENTAL SET-UP

The experiments were performed in an open recirculating water channel at the Turbulence and Hydraulic Engineering Laboratory (THEL) at the University of Manitoba. The streamwise length, spanwise width, and vertical height of the channel are 6.0 m, 0.6 m, and 0.45 m, respectively. A rectangular prism with thickness, $h$ = 20 mm, chord length, $C$ = 120 mm (corresponding to CR = 6), and spanwise width, $B$ = 588 mm was used. The water depth was $H$ = 420 mm, and the prism was installed horizontally, 210 mm above the bottom wall. The spanwise aspect ratio ($B/h$) was 29.4 and the blockage ratio ($h/H$) was 4.8%. Van Veen et al. (2025) investigated the effects of Reynolds number (Re) on a CR = 6 prism and demonstrated that the flow characteristics are independent of Reynolds number for Re ≥ 10000. Based on this finding, the freestream velocity was set to 0.5 m/s, and the Reynolds number was 10000, to isolate its effect. The turbulence intensity measured at the mid-height of the channel and in the absence of the prism was 2%.

To achieve the desired FST intensities, two passive grids - a regular grid and a fractal grid, were manufactured from a 6.35 mm stainless steel and positioned at the inlet of the test section. The blockage ratios of the grids are 35% and 41%, respectively. Schematics of the grids are shown in Figure 1. Detailed geometric specifications and flow characteristics downstream of the grids are provided in Sagharichi and Tachie (2025). The distance between the grids and the leading edge of the prism was 2380 mm, where the turbulence is homogenous and isotropic. The FST intensities generated at the location of the leading edge, without the prism installed, were Tu = 5% and 13% for the regular and fractal grids, respectively. The corresponding integral length scales for the regular and fractal grids were 1.0$h$ and 1.7$h$, respectively. According to Bearman and Morel (1983) and Haan et al. (1998), the length scales do not have significant influence on the flow dynamics if the length scale is between 0.4$h$ and 4$h$. Therefore, the flow is not significantly affected by length scales.

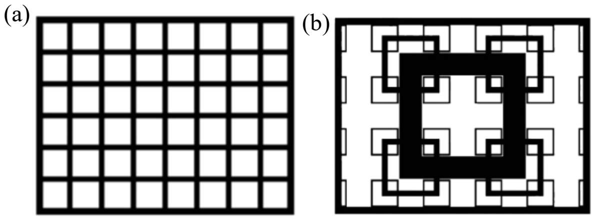


Figure 1: Schematic of the turbulence grids. (a) regular and (b) fractal grids.

Time-resolved particle image velocimetry was used to perform velocity measurements in the $x$-$y$ plane at the mid-span of the channel. The water was seeded with silver coated hollow glass spheres with mean diameter of 10 µm and density of 1400 kg/m$^3$. A diode pumped dual-cavity dual-head high speed Neodymium-doped yttrium lithium fluoride laser was used to illuminate the seeding particles. Two high-speed 12-bit complementary metal oxide semiconductor cameras, with resolution of 2560 pixel × 1600 pixel were positioned side by side to image the flow as shown in Figure 2. The first camera was fitted with a Sigma 105 mm lens to provide higher spatial resolution to adequately resolve the small-scale dynamics of the separated shear layer and the second camera was fitted with a Nikon 60 mm lens. The dimensions of the first field of view (FOV) were set to 6.0$h$ × 3.8$h$ in the streamwise and vertical direction, respectively, and the second FOV were 14.3$h$ × 8.9$h$. For each test case, the sampling frequency was set to 800 Hz and 60000 images were captured. A commercial software (Davis version 10.0.5) supplied by LaVision Inc. was used for data acquisition and image post-processing. Velocity vector calculations were performed using a GPU-accelerated multi-pass cross-correlation algorithm with an initial interrogation window of 128 pixel × 128 pixel with 50% overlap and four additional passes with interrogation window of 24 pixel × 24 pixel with 75% overlap.

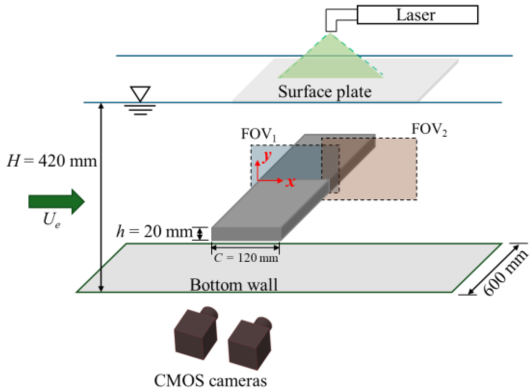


Figure 2: Schematic of the experimental setup.

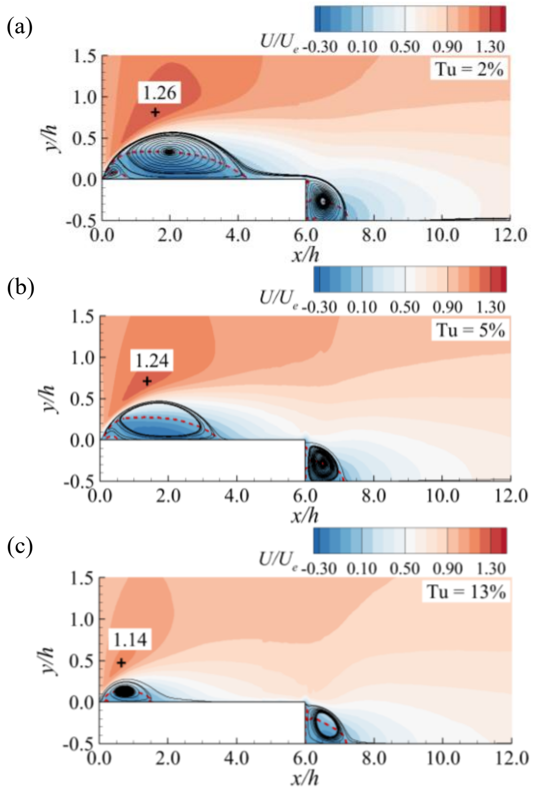


Figure 3: Contours of the streamwise mean velocity ($U$) superimposed with mean streamlines and the isopleth of $U$ = 0 for (a) Tu = 2%, (b) Tu = 5%, and (c) Tu = 13%.

## RESULTS AND DISCUSSION

### Mean flow characteristics

Figure 3 shows contours of the streamwise mean velocity ($U$) superimposed with mean streamlines and isopleth of $U$ = 0 to visualize the mean flow topology and demarcate the reverse flow regions. Regardless of FST intensity, the incoming flow separates at the sharp leading edge of the prism and deflects upward into the uniform flow. The flow accelerates over the prism, resulting in a local maximum velocity. The mean streamlines reveal the formation of recirculation regions over and in the wake region of the prism, referred to as primary and wake vortices, respectively. A relatively small recirculation bubble, referred to as the secondary vortex, forms within the primary bubble close to the leading edge. This secondary vortex forms due to an adverse pressure gradient generated by the decelerating flow within the primary recirculation bubble. The secondary bubble is only present for Tu = 2% and 5%, and the streamwise lengths of the bubbles are 0.81 and 0.56, respectively. For Tu = 13%, however, the secondary vortex is suppressed due to the reduced streamwise deceleration of the near-wall mean flow which weakens the local adverse pressure gradient necessary to form the secondary vortex. The reattachment length of the primary vortex, defined as the streamwise distance from the leading edge to the point where the isopleth of $U = 0$ intersects with the top surface of the prism, is $x_p/h$ = 4.26, 3.45, and 1.50 for Tu = 2%, 5%, and 13%, respectively, corresponding to an overall reduction of 64.8%. The decrease in size of the separation bubble is consistent with previous observations (Kiya and Sasaki, 1983) and was attributed to the rapid recovery of the surface pressure due to increased entrainment of high-momentum fluid from the outer flow into the recirculation bubble. The wake recirculation length, measured as the streamwise distance from the trailing edge to the saddle point is $x_w/h$ = 1.2, regardless of the tested FST intensities. The progressive attenuation of the incoming turbulence along the prism surface and the shielding effect of the body limits the direct influence of FST on the wake recirculation region. Similar FST intensity independence in the wake was reported by Zhu et al. (2020) and Li et al. (2021) for prisms with CR = 5 and 6, respectively.

**Frequency spectra**

The effects of FST on the shear layer instabilities and wake vortices are examined using the frequency spectra of the velocity fluctuations. To detect the Kelvin-Helmholtz (KH) frequency, spectra analysis of the streamwise velocity fluctuation is performed at selected locations along the shear layer and presented in Figure 4. The KH instabilities occur as broadband peaks at relatively high frequencies as the separated flow transitions to turbulence (Moore et al., 2019). For Tu = 2% (Figure 4a), a broadband peak is observed at a Strouhal number $St_{KH}$ (= $f_{KH}h/U_e$, where $f_{KH}$ is the KH frequency) of 2.07. As the flow evolves downstream, the characteristic KH frequency decreases due to the merging of the shed vortices. For Tu = 5% (Figure 4b), the KH instability remains detectable at a Strouhal number of 2.60; however, the associated spectral peak becomes narrower and less energetic compared to Tu = 2%. The spectra for Tu = 2% and 5% also reveal peaks at frequencies that are an order of magnitude lower than $St_{KH}$. Meanwhile for Tu = 13% (Figure 4c), the spectra reveal dominant peak at a low frequency of St = 0.037 and no distinct high-frequency broadband peak is observed, suggesting a bypass of the KH instability. A similar bypass of transition was observed by Langari and Yang (2013) and Lander et al. (2016) for a flat plate and a square prism, respectively.

The wake or VK vortex shedding frequency is determined using the frequency spectra of the vertical velocity fluctuations at the location of maximum vertical Reynolds normal stress in the wake region (Figure 5). Regardless of the FST intensity, the spectra reveal a distinct peak at Strouhal number $St_{VK}$ (= $f_{VK}h/U_e$, where $f_{VK}$ is the VK frequency) of 0.16, which is in good agreement with 0.159 reported in literature for the CR = 6 prism (Liu and Zhang, 2015). The contrasting response of the shear layer (KH) and wake (VK) instabilities to FST intensity arises from their fundamentally different instability mechanisms, as well as the chord-to-thickness ratio of the prism. The Kelvin-Helmholtz instability is a local, convective instability whose growth is sensitive to initial shear layer thickness and its receptivity to upstream disturbances and is therefore strongly influenced by FST intensity. In contrast, von Kármán vortex shedding is a global instability governed by the near wake structures, whose characteristic frequency is insensitive to the variation in FST intensity.

The relative influence of the Kelvin-Helmholtz and von Kármán vortices is often examined using their frequency ratio. This ratio, $f_{KH}/f_{VK}$, is 13 and 16 for Tu = 2% and 5%, respectively. These values are significantly lower than 75 and 37 reported for prisms with CR = 1 and 5, respectively (Moore et al., 2019). These results indicate a reduced level of interaction between the KH and VK vortices with increasing CR. It is noted that, in contrast to rectangular prisms with CR ≤ 5, the spectra along the shear layer (Figure 4) do not show the signature of the VK frequency, further reinforcing the notion that the influence of the wake dynamics for a prism with CR = 6 does not extend to the leading edge.

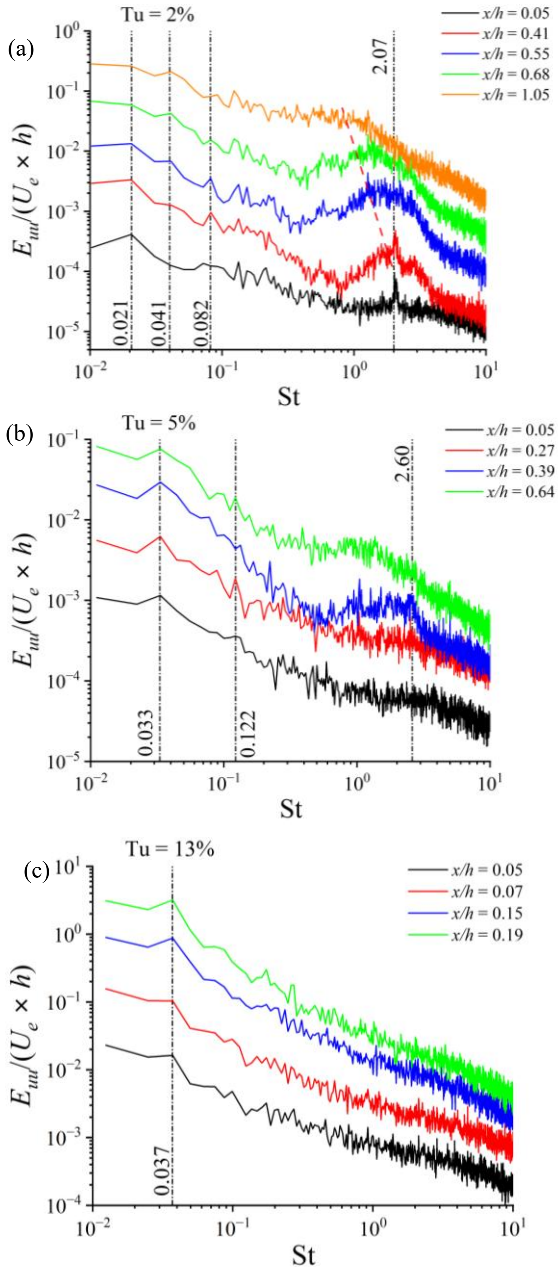


Figure 4: Frequency spectra along the shear layer for (a) Tu = 2%, (b) Tu = 5%, and (c) Tu = 13%.

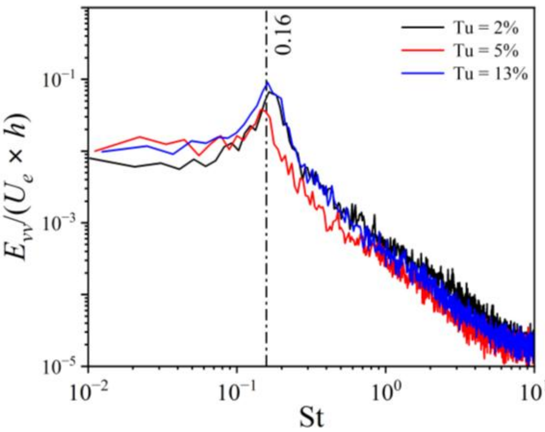


Figure 5: Frequency spectra at the location of maximum vertical Reynolds normal stress for all the test cases.

**Reverse flow area**

The quasi-periodic expansion and shrinkage of the recirculation region over the surface of the prism is investigated using the instantaneous reverse flow area to determine the large-scale flapping motions. Following the procedure proposed by Pearson et al. (2013), the instantaneous reverse flow area ($A$) was determined by summing up areas with negative instantaneous streamwise velocity ($u < 0$) within the region over the prism ($x/h \times y/h \in [0.0, 6.0] \times [-0.5, 1.5]$). The mean reverse flow area was $\bar{A}/h^2 = 1.04, 0.74$, and $0.24$, for Tu = 2%, 5%, and 13%, respectively, showing a monotonic decrease with FST intensity. The frequencies associated with the flapping motion of the recirculation bubble are examined using the frequency spectra of the reverse flow area shown in Figure 6. The spectra reveal dominant frequencies at $St_{FM}$ ($= f_{FM}h/U_e$, where $f_{FM}$ is the flapping motion frequency) of 0.040, 0.044, and 0.037 for Tu = 2%, 5%, and 13%, respectively, which correspond to $St_{LT}$ 0.17, 0.15, and 0.06. These frequencies are in good agreement with the flapping frequency of $St_{LT}$ ($= f_{FM}L_T/U_e$, where $L_T$ is the reattachment length) of $0.08 - 0.20$ reported in the literature for rectangular prisms (Kiya and Sasaki, 1983; Fang et al., 2022; Abdul-Salam et al., 2024; Cimarelli et al., 2024).

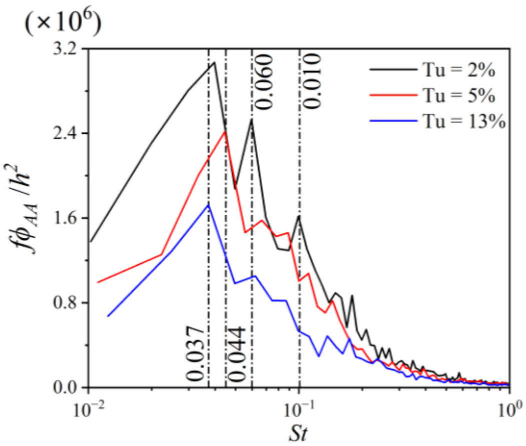


Figure 6: Frequency spectra of the reverse flow area.

**Spectral decomposition of the Reynolds stresses**

The spectra analysis examined using the velocity fluctuations and the reverse flow area revealed the signatures of the different instabilities in the flow. These instabilities are associated with different scales of motions and contribute differently to the overall vortex dynamics. The influence of FST on the relative contributions of these instabilities to the total streamwise Reynolds normal stress ($\overline{u'u'}$) and the Reynolds shear stress ($\overline{u'v'}$) is examined in Figures 7 and 8, respectively. It should be noted that the analysis of the vertical Reynolds normal stress ($\overline{v'v'}$) is not presented for brevity. The turbulence motions are partitioned into three frequency bands, based on the frequencies identified from the spectra of the velocity and reverse flow area to characterize the dynamics associated with the small-scale KH, intermediate-scale VK, and large-scale flapping motions. The boundaries of each band are determined from the onset of each dominant spectral peak, and the resulting frequency ranges are summarized in Table 1.

Table 1. Summary of the frequency bands

| FST (%) | Small | Intermediate | Large |
|---|---|---|---|
| 2.0 | 0.82 to 15 | 0.10 to 0.82 | 0 to 0.10 |
| 5.0 | 2.30 to 15 | 0.10 to 2.30 | 0 to 0.10 |
| 13.0 | 4.24 to 15 | 0.10 to 4.24 | 0 to 0.10 |

Contours of the total streamwise Reynolds normal stress ($\overline{u'u'}$) are presented in Figure 7(a, b, c) to examine the effects of FST level on the turbulence characteristics. Regardless of the FST level, elevated regions of total $\overline{u'u'}$ are observed along the separated shear layer. The total $\overline{u'u'}$ reveals two peaks; one along the shear layer, which intensifies as FST intensity increases, and another in the wake which is independent of FST intensity. For Tu = 2%, the contributions from the small-scale motions show elevated $\overline{u'u'}$ over the surface of the prism, highlighting the influence of the KH instability on the shear layer over the body. The small-scale contributes about 56% to the total peak stress over the prism. The intermediate- and large-scales show similar contributions both over and in the wake of the prism. As FST intensity increases to 5%, the magnitude and spatial extent of the contributions from the small-scale are reduced, suggesting a suppression of the KH instability. Meanwhile, the intermediate- and large-scales show similar contributions both over and in the wake, similar to Tu = 2%. At Tu = 13%, the contributions from the small scales are significantly weakened. This observation is consistent with the results in Figure 4, where the signature of the KH instabilities diminishes with increasing FST intensity. The intermediate scales contribute both over the prism and in the wake but the contributions in the wake are more pronounced. In contrast, the dynamics of the large scales are primarily concentrated over the surface with negligible contributions in the wake. Kiya and Sasaki (1983) noted that increasing FST induces large-scale vortices, consistent with the present observation of more energetic structures at higher FST level.

Contours of the total Reynolds shear stress ($\overline{u'v'}$) presented in Figure 8(a, b, c) show elevated regions of negative $\overline{u'v'}$ concentrated along the shear layers. As FST increases to 13%, $\overline{u'v'}$ intensifies and shifts towards the wall of the prism. Regardless of the FST intensity, the Reynolds shear stress is positively signed very close to the leading edge and within the wake vortex. The positive region near the leading edge is a consequence of the misalignment between the Cartesian coordinate system and the mean streamline (Fang and Tachie, 2020). The small-scale contribution to $\overline{u'v'}$ exhibits trends similar to those observed for $\overline{u'u'}$, with contributions concentrated over the surface of the prism at low FST intensity that weaken as the FST intensity increases. For Tu = 2% and 5%, the contributions from the intermediate scales are significant over the prism surface and also in the wake, while the large scales contribute comparatively less. In contrast, for Tu = 13%, the intermediate scales dominate the wake, whereas the intermediate and large scales contribute similarly over the prism surface.

## SUMMARY AND CONCLUSION

In this study, the influence of freestream turbulence intensity on the turbulent flow around intermediate rectangular prism with chord-to-thickness ratio of 6 was experimentally investigated using time-resolved particle image velocimetry at a Reynolds number of 10000. Two passive grids were used to generate FST intensity of 5% and 13% and the results were compared with a base FST intensity of 2% (without grid).

Analysis of the mean flow reveal an overall reduction of 65% in the recirculation length of the primary vortex with increase in FST intensity. The secondary vortex shows a 31% reduction when the Tu increased to 5% but is suppressed for Tu = 13%. The wake vortex, on the other hand is independent of the FST intensity.

Frequency analysis of the fluctuating velocities and reverse flow area reveal the presence of three distinct instabilities: small-scale Kelvin-Helmholtz (KH) instabilities, intermediate-scale vortex shedding, and large-scale flapping motions. Along the shear layer, the spectra show the occurrence of KH instability at Tu = 2% and 5% but is bypassed when FST intensity is increased to 13%. In contrast, the wake vortex shedding frequency shows no variation with changes in the FST intensity. Spectral decomposition was employed to investigate the relative contributions of the various instabilities to the Reynolds stresses. The results show that the small scales contribution to Reynolds stresses is concentrated over the surface of the prism at low FST intensity and weakens as the FST intensity increases. For Tu = 2% and 5%, both the intermediate and large scales contribute to $\overline{u'u'}$ but the intermediate scales are the dominant contributors to $\overline{u'v'}$. For Tu = 13%, the intermediate scales dominate $\overline{u'u'}$ in the wake, while the large scales dominate $\overline{u'u'}$ over the surface of the prism.

## ACKNOWLEDGEMENT

The authors are grateful to the Natural Sciences and Engineering Research Council of Canada (NSERC) for their financial support. We are also grateful to Canada Foundation for Innovation (CFI) for funding the experimental facility.

## REFERENCES

Abdul-Salam, F. B., Fang, X., and Tachie, M. F., 2024, "Influences of blockage ratio and Reynolds number on the spatiotemporal dynamics around a rectangular prism", *Physics of Fluids*, 36, 105198.

Bearman, P. W., and Morel, T., 1983, "Effect of free stream turbulence on the flow around bluff bodies", *Progress in Aerospace Sciences,* 20(2-3), 97–123.

Cimarelli, A., Corsini, R., and Stalio, E., 2024, "Reynolds number effects in separating and reattaching flows with passive scalar transport", *Journal of Fluid Mechanics*, 984.

Fang, X., and Tachie, M. F., 2020, "Spatio-temporal dynamics of flow separation induced by a forward-facing step submerged in a thick turbulent boundary layers", *Journal of Fluid Mechanics*, 892, A40.

Fang, X., Tachie, M. F., and Dow, K., 2022, "Turbulent separations beneath semi-submerged bluff bodies with smooth and rough undersurface", *Journal of Fluid Mechanics*, 947.

Haan, F. L., Kareem, A., and Szewczyk, A. A., 1998, "The effects of turbulence on the pressure distribution around a rectangular prism", *Journal of Wind Engineering and Industrial Aerodynamics*, 77-78, 381–392.

Kiya, M., and Sasaki, K., 1983, "Freestream turbulence effects on a separation bubble", *Journal of Wind Engineering and Industrial Aerodynamics*, Vol. 14, pp. 375- 386.

Kumahor, S., and Tachie, M. F, 2023, "Effects of streamwise aspect ratio on the spatio-temporal characteristics of flow around rectangular cylinders", *International Journal of Heat and Fluid Flow*, Vol. 101, 109133.

Lander, D. C., Letchford, C. W., Amitay, M., and Kopp, G. A., 2016, "Influence of the bluff body shear layers on the wake of a square prism in a turbulent flow", *Physical Review Fluids*, Vol. 1, 044406.

Langari. M., and Yang, Z., 2013, "Numerical study of the primary instability in a separated boundary layer transition under elevated free-stream turbulence", *Physics of Fluids*, 25.

Li, M., Li, Q., Shi, H., and Li, M., 2022, "Effects of free-stream turbulence on the near wake flow and aerodynamic forces of a square cylinder", *Journal of Fluids and Structures,* 114, 103748.

Li, W., Patruno, L., Niu, H., de Miranda, S., and Hua, X., 2021, "Aerodynamic admittance of a 6:1 rectangular cylinder: A computational study on the role of turbulence intensity and integral length scale", *Journal of Wind Engineering and Industrial Aerodynamics,* 218, 104738.

Liu, Y., and Zhang, Q., 2015, "Dynamic mode decomposition of separated flow over a finite blunt plate: Time-resolved particle image velocimetry measurements", *Experiments in Fluids,* 56 (7).

Moore, D. M., Letchford, C. W., and Amitay, M., 2019, "Energetic scales in a bluff body shear layer", *Journal of Fluid Mechanics*, Vol. 875, pp. 543- 575.

Okajima, A., 1982, "Strouhal Numbers of Rectangular cylinders", *Journal of Fluid Mechanics*, Vol. 123, pp. 379-398.

Pearson, D.S, Goulart, P.J., Ganapathisubramani, B., 2013, "Turbulent separation upstream of a forward-facing step", *Journal of Fluid Mechanics*, Vol. 724.

Sagharichi, A., and Tachie, M. F, 2025, "Analysis of non-equilibrium turbulence dissipation downstream of regular and fractal grids in an open channel flow", *International Journal of Heat and Fluid Flow*, Vol. 114, ,109822.

Van Veen, E., Abdul-Salam, F. B., and Tachie, M. F., 2025, "Dynamics of separated flow over a rectangular prism with chord-to-thickness ratio of 6 at moderate Reynolds numbers", *Proceedings of the ASME FEDSM 2025*, Philadelphia, USA.

Zhao, C., Wang, H., Zeng, L., Alam, M. M., and Zhao, X., 2021, "Effects of oncoming flow turbulence on the near wake and forces of a 3D square cylinder", *Journal of Wind Engineering and Industrial Aerodynamics,* 214, 104674.

Zhu, G., Huang, S., and Li, Q. S., 2020, "Large-eddy simulation of the inflow turbulence transport and aerodynamics of a rectangular 5:1 cylinder with high-order numerical methods", *Journal of Wind Engineering and Industrial Aerodynamics,* 207, 104366.

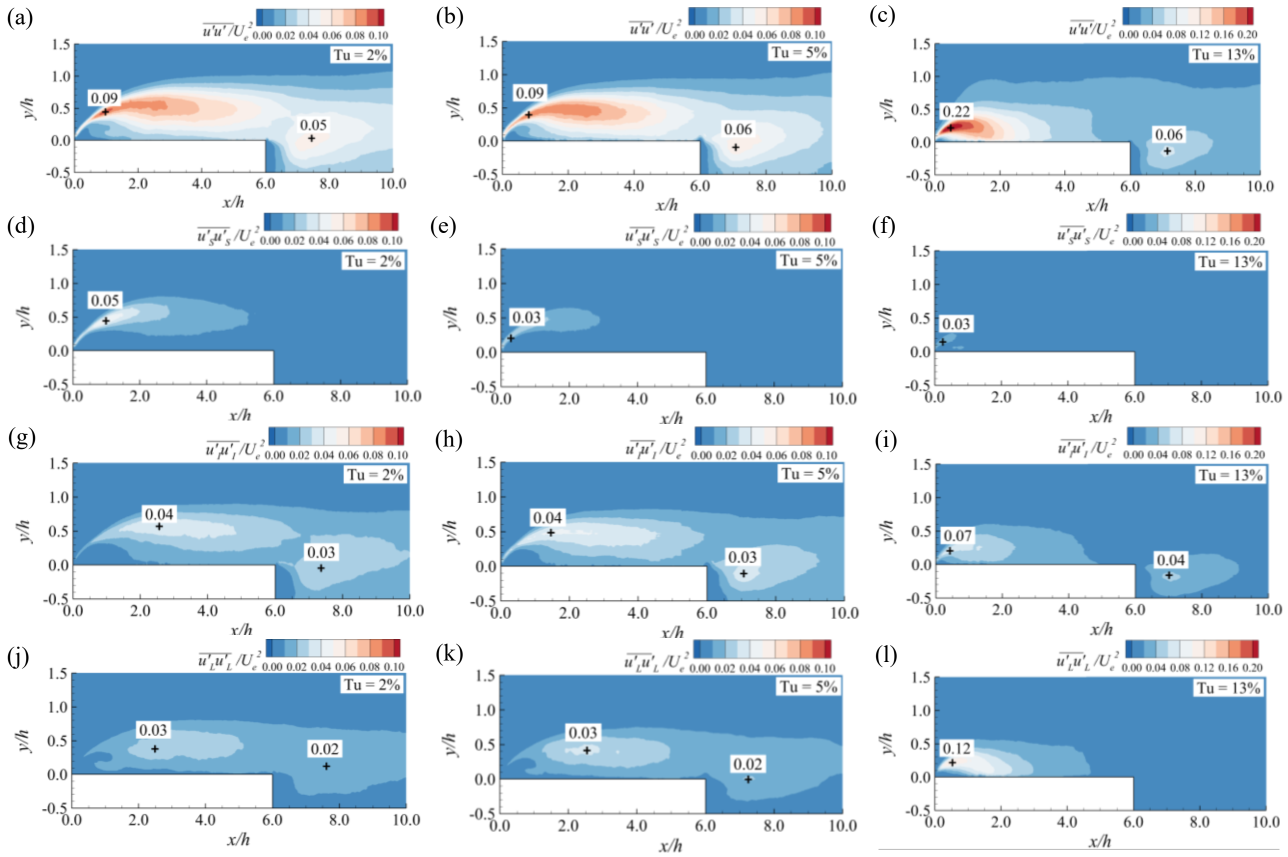


Figure 7: Contours of the total and decomposed streamwise Reynolds normal stresses for Tu = 2% (top), Tu = 5% (middle), and Tu = 13% (bottom).

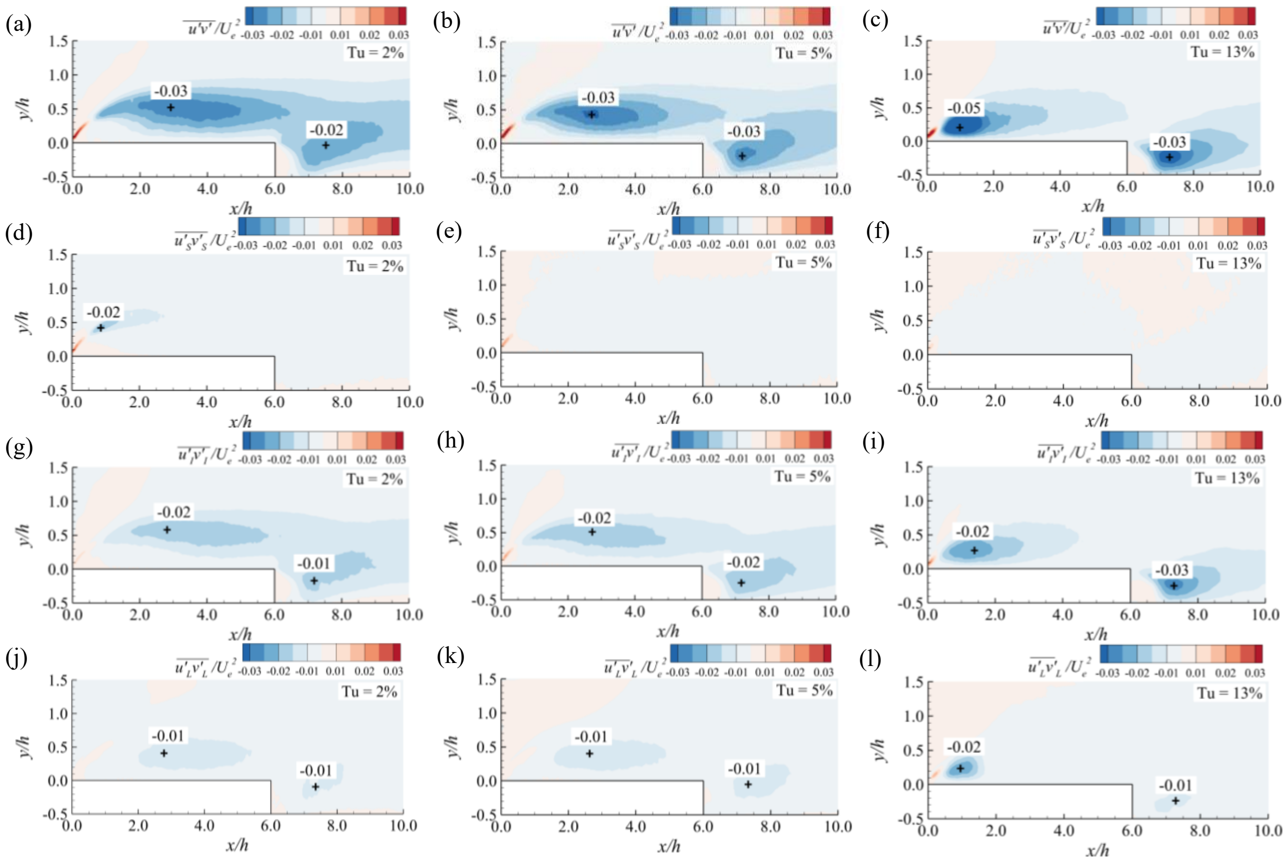


Figure 8: Contours of the total and decomposed Reynolds shear stresses for Tu = 2% (top), Tu = 5% (middle), and Tu = 13% (bottom).